

Effect of a Magnetic Field in Simulating the Plume-Field of an Anode Layer Hall Thruster

Yongjun Choi¹

University of Michigan, Ann Arbor, MI 48109

Michael Keidar²

The George Washington University, Washington DC 20052

and

Iain D. Boyd³

University of Michigan, Ann Arbor, MI 48109

Two dimensional axi-symmetric simulations of xenon plasma plume flow fields from a D55 anode layer Hall thruster are performed with a hybrid particle-fluid method. The magnetic field surrounding the Hall thruster exit is included in the calculation. In this simulation, the Boltzmann model and a detailed fluid model are used to compute the electron properties, the direct simulation Monte Carlo method models the collisions of heavy particles, and the Particle-In-Cell method models the transport of ions in an electric field. The accuracy of the simulation is assessed through comparison with various measured data. It is found that a magnetic field significantly affects the profile of the plasma in the Detailed model. For instance, in the case of zero magnetic field, the plasma has a potential about 110V at 10 mm from the thruster exit, while in the case of a magnetic field included, the plasma potential is about 80V. Results predicted by the Detailed model with the magnetic field are found to be in better agreement with experimental data.

Nomenclature

\mathbf{B}	= magnetic field vector	T_H	= heavy particle temperature
c_e	= mean electron thermal velocity	$\mathbf{V}_{\text{drift}}$	= electron drift velocity vector
C_i	= ionization coefficient	\mathbf{V}_e	= electron velocity vector
\mathbf{E}	= electric field vector	\mathbf{V}_i	= ion velocity vector
e	= unit charge	σ	= plasma conductivity
g	= relative velocity	σ_j	= reference cross section for xenon ionization
k	= Boltzmann constant	ε_i	= ionization energy
m_e	= electron mass	k_e	= electron thermal conductivity
m_i	= ion mass	ν_e	= electron collision frequency
n_a	= atom number density	ν_{ei}	= ion-electron collision frequency
n_e	= electron number density	ν_{en}	= neutral electron collision frequency
n_{max}	= local maximum of number density	ϕ	= plasma potential
p_e	= electron pressure	Ψ	= electron stream function
T_e	= electron temperature		

¹ Graduate student, Department of Aerospace Engineering, AIAA Student Member.

² Assistant Professor, Mechanical and Aerospace Engineering, AIAA Senior Member.

³ Professor, Department of Aerospace Engineering, AIAA Associate Fellow.

I. Introduction

Hall effect thrusters represent an efficient form of electric propulsion devices for applications requiring low thrust levels, e.g. station-keeping, orbit raising, and orbit transfer. In a Hall thruster, ions are accelerated by electric fields and used to generate propulsive thrusts. The energy required to accelerate ions is obtained from on-board batteries or solar cells. Hall thrusters provide better performance than chemical propulsion systems because they obtain electric power input directly in space through solar cells, do not need to carry any oxidizer, and so allow a larger payload. Furthermore, Hall thrusters can realize much higher propellant exhaust velocities than chemical propulsion systems, thereby achieving higher impulse from a given propellant mass and making the use of Hall thrusters for interplanetary missions attractive.

Two types of Hall thrusters have been developed: a thruster with closed electron drift and extended acceleration zone, or Stationary Plasma Thruster (SPT), and a thruster with a very short acceleration channel, or Thruster with Anode Layer (TAL). The SPT employs a relatively long acceleration channel and ceramic wall insulator materials, such as boron nitride or silicon carbide. The TAL employs a shorter acceleration channel and conducting metallic wall materials which are typically stainless steel or molybdenum.

Among Hall thruster technologies, TAL, which was developed in the 1960's at TsNIIMASH, seems to be advantageous for two reasons. First, TAL has a very short acceleration zone (a few millimeters) and so there is less contact of ions with thruster surfaces; hence, it is favorable for long-term missions because of a reduction in erosion of thruster components. Second, higher power Hall thrusters will be needed in future space missions and a TAL with very high power has been specially developed to meet this requirement.¹

Modeling of the plume fields of Hall thrusters yields important information in two different ways. First, it provides understanding of the plume impingement that involves fluxes of high-energy ions and charge-exchanged particles onto sensitive spacecraft devices such as solar arrays. Second, plume modeling helps to clarify the complex plasma processes inside the thruster with the aim of improving propulsion performance. The near field plume of a Hall thruster is a very important region because its high plasma density facilitates the use of a variety of experimental diagnostic techniques. Such diagnostics are much more difficult to apply either in the internal thruster flow or in the plume far field. Therefore, understanding the behavior of the thruster plume is critical to the design of thrusters and spacecraft.

In the Hall thruster, the magnetic field in the acceleration channel provides the closed azimuthal electron drift and enhances the impact ionization of the propellant. Experimental measurements of the near-field plasma plume from Hall thrusters show that the magnetic field leaks into the plume and is strong enough to affect the electron motion in the near-field plume region.^{2, 3} However, among the rare reports of simulations for plume flows from a TAL, very few considered magnetic field effects. One of these reports performed quasi one dimensional simulations of the plasma plume from the D55 and indicated that the plasma potential increased with axial distance from the thruster exit plane.⁴

A plasma plume is a complex rarefied flow with several species: atoms, positively charged ions, and electrons. Generally, a hybrid particle-fluid approach is used for the computational simulation of plasma plume flow into vacuum. The direct simulation Monte Carlo (DSMC) method⁵ simulates the collisions of heavy particles (ions and atoms), and the Particle-In-Cell (PIC) technique⁶ models the transport of ions in electric fields. Electrons are treated using a fluid description, because electrons, which have significantly lighter mass, can adjust their velocities more quickly than ions or atoms.

For the electron fluid model, usually the *Boltzmann* relation is adopted.^{7, 8} The *Boltzmann model* provides the plasma potential using several strong assumptions such as a constant electron temperature for the whole domain. The *Detailed model* which has been developed recently,⁹ is based on the conservation laws for electrons and is capable of representing accurate and detailed distributions for electron temperature, plasma potential and electron velocity. This model was successfully applied in a simulation of an axi-symmetric plasma plume from a 200W class SPT-type Hall thruster⁹ and in another simulation of 3D plasma plumes from a cluster of four 200 W class Hall thrusters.¹⁰

In this study, we analyze the possible influence of the magnetic field on the plasma plume. The 2D axi-symmetric plume flow fields from a D55 TAL Hall thruster are investigated using MONACO,¹¹ a hybrid PIC-DSMC code developed at the University of Michigan with both the *Boltzmann model* and the *Detailed model*. A stationary magnetic field is assumed.

The device considered in the present study is the D55 TAL Hall thruster developed by TsNIIMASH. We have chosen to study the D55 Hall thruster because of the availability of a significant amount of experimental data for this device.

Section II reviews numerical models, and brief information for experiments and flow conditions. Section III presents general features of the numerical 2D simulation results and a comparison of these results with experimental data taken in the plume of the D55.

II. Models and Flow Conditions

A. Plasma Dynamics

For particle simulation of plume flows, heavy neutrals and ions are modeled with the PIC-DSMC method, and the electrons are assumed as a fluid because electrons adjust their velocities more quickly with their significantly lighter mass.

The simplest fluid electron model is the *Boltzmann* relation

$$\phi = \phi_{ref} + \frac{kT_{ref}}{e} \ln \left(\frac{n_e}{n_{ref}} \right) \quad (1)$$

This equation is derived from the electron momentum equation using several assumptions including that the electron flow is isothermal, collisionless, obeys the ideal gas law, and the magnetic field is neglected.

Recently, the *Detailed model* was proposed⁹ which represents a significantly increased level of physics compared to the *Boltzmann model*. In the *Detailed model*, the electron continuity equation is transformed into a Poisson equation by assuming steady flow and introducing a stream function;⁹

$$\nabla^2 \Psi = C_i n_e n_a \quad (2)$$

where $n_e \mathbf{V}_e = \nabla \Psi$ and the xenon ionization rate coefficient C_i is expressed as a function of electron temperature using a relation proposed by Ahedo¹²

$$C_i = \sigma_i c_e \left(1 + \frac{T_e \varepsilon_i}{(T_e + \varepsilon_i)^2} \right) \exp \left(-\frac{\varepsilon_i}{T_e} \right) \quad (3)$$

In the presence of a magnetic field, assuming a steady state, neglecting the inertial term, the electron momentum equation is written¹³

$$0 = -en_e (\mathbf{E} + \mathbf{V}_e \times \mathbf{B}) - \nabla p_e + n_e v_e m_e (\mathbf{V}_e - \mathbf{V}_i) \quad (4)$$

Experimental investigation of the magnetic field distribution near a Hall thruster shows that the magnetic field has both radial and axial components of which the radial component is much larger.³ Thus, for simplicity, only the radial component of the magnetic field is considered. In this case, the plasma plume flow is across the magnetic field and the radial component of the magnetic field B varies along the axis. With another assumption that electrons behave as an ideal gas, Eq. (4) can be written in component form as:

$$0 = -en_e (E_z - V_{e\phi} B_r) - kT \frac{dn_e}{dz} - n_e v_e m_e (V_{ez} - V_{iz}) \quad (5)$$

$$0 = -en_e (E_z - V_{e\phi} B_r) - kT \frac{dn_e}{dz} - n_e v_e m_e (V_{ez} - V_{iz}) \quad (6)$$

From the azimuthal component,

$$V_{e\phi} = -\frac{e}{m_e v_e} V_{ez} B_r + V_{i\phi} \approx -\frac{e}{m_e v_e} V_{ez} B_r \quad (7)$$

However, $V_{e\phi}$ from Eq. (7) is derived for the case where the density is high enough to produce a significant collision rate. If the density is low, then collisions are very rare, and $V_{e\phi}$ becomes just a drift velocity,

$$V_{drift} = E_z / B_r.$$

Here we use a combination of these two limiting results:

$$V_{e\phi} = (1-w)V_{drift} + w \left(-\frac{e}{m_e v_e} V_{ez} B_r \right) \quad (8)$$

where the weight function is $w = \left(\frac{n}{n_{\max}} \right)$ and n_{\max} is a local maximum which is chosen as the neutral particle

density at the thruster exit.

A generalized Ohm's law is obtained from Eq. (4)

$$\nabla \cdot \mathbf{j} = \nabla \cdot \boldsymbol{\sigma} \left[-\nabla \phi + \mathbf{V}_e \times \mathbf{B} + \frac{1}{en_e} \nabla (n_e kT_e) \right] \quad (9)$$

where $-\nabla\phi = \mathbf{E}$.

From Eq. (9), an equation for the plasma potential can be obtained

$$\begin{aligned} \nabla \cdot (\sigma \nabla \phi) &= \frac{k\sigma}{e} \left(\nabla^2 T_e + T_e \nabla^2 (\ln n_e) \right) + \sigma \nabla (\ln n_e) \cdot \nabla T_e + T_e \nabla \sigma \cdot \nabla (\ln n_e + \nabla \sigma \cdot \nabla T_e) \\ &- \frac{\partial \sigma}{\partial z} V_\phi B_r - \sigma \left[V_\phi \frac{\partial B_r}{\partial z} + B_r \frac{\partial V_\phi}{\partial z} \right] \end{aligned} \quad (10)$$

For given n_e , v_e , T_e , and V_ϕ the charge continuity condition

$$\nabla \cdot \mathbf{j} = 0 \quad (11)$$

is solved to obtain the plasma potential.

The electron temperature equation is obtained from the steady state electron energy equation¹⁴

$$\nabla^2 T_e = -\nabla \ln \kappa_e \cdot \nabla T_e + \frac{1}{\kappa_e} \left(-\mathbf{j} \cdot \mathbf{E} + \frac{3}{2} n_e (\mathbf{V}_e \cdot \nabla) k T_e + p_e \nabla \cdot \mathbf{V}_e + 3 \frac{m_e}{m_i} v_e n_e k (T_e - T_H) + n_e n_a C_i \varepsilon_i \right) \quad (12)$$

Finally, the electron conductivity σ and the electron thermal conductivity κ_e can be evaluated using their basic definitions¹⁴

$$\sigma = \frac{e^2 n_e}{m_e v_e} \quad (13)$$

$$\kappa_e = \frac{2.4}{1 + \frac{v_{ei}}{\sqrt{2}v_e}} \frac{k^2 n_e T_e}{m_e v_e} \quad (14)$$

where $v_e = v_{ei} + v_{en}$, v_{ei} is the ion-electron collision frequency, v_{en} is the neutron-electron collision frequency and these frequencies are evaluated for the xenon system using cross sections provided in ref. 14.

By treating the right hand side terms as known sources and solving Eqs. (2), (11) and (12) three fundamental fluid electron properties are obtained, i.e., electron velocity, plasma potential, and electron temperature.

B. Collision Dynamics

Two types of collisions are important in the Hall thruster: elastic (momentum exchange: MEX) and charge exchange (CEX). There are two kinds of elastic collisions: atom-atom and atom-ion interactions. For atom-atom collisions, the Variable Hard Sphere⁵ model is used and the collision cross section for xenon is

$$\sigma_{el}(\mathbf{Xe}, \mathbf{Xe}) = \frac{2.12 \times 10^{-18}}{g^{2\omega}} \quad (15)$$

where g is the relative velocity and $\omega=0.12$ is related to the viscosity temperature exponent for xenon. For atom-ion elastic collisions, the MEX cross section is set equal to the CEX cross section.

Charge exchange concerns the transfer of one or more electrons between an atom and an ion. For single charged ions, we use the following cross section measured by Pullins et al.¹⁵ and Miller et al.¹⁶

$$\sigma_{cex}(\mathbf{Xe}, \mathbf{Xe}^+) = 1.1872 \times 10^{-20} (142.21 - 23.30 \log(g)) \quad (16)$$

Also, Refs. 15 and 16 reported that the CEX cross section for double charged ions is approximately half as large as single charged ions at corresponding energies.

C. Flow Conditions

A schematic of the D55 thruster is presented in Fig. 1. The D55 thruster has an annular anode chamber with a mean diameter of 55 mm and a width of 5 mm.

Figure 2 shows contours of the radial component of the magnetic field outside of the thruster which are reconstructed using experimental data.² We extrapolated data from 0 mm to 5 mm where experimental data are not available. Because of the proprietary nature of the magnetic field data, the values reported in this paper have been normalized to the maximum value.

We consider three different experimental conditions. Most of the results presented here are for a series of experiments conducted at the University of Michigan.² The D55 thruster was operated at a flow rate of 4.76 mg/s of xenon, a discharge voltage of 300 V, and a current of 4.5 A. The specific impulse under these conditions was previously measured to be 1,810 s.¹⁷ When a thruster exit velocity is chosen consistent with measurements of plasma potential and ion velocity data, this corresponds to the case where about 80% of the thrust is generated inside the thruster. The number fraction of double xenon ions is assumed to be 0.25. At the thruster exit, the electron temperature is taken to be 10 eV in the *Boltzmann model* and the *Detailed model* to obtain good agreement between

the simulations and the data measured in the plume field. The temperature of the ions is assumed to be 4 eV, and that of the neutrals is assumed to be 750 K. The backpressure in the Michigan facility is reported as 8.3×10^{-3} Pa.

The second flow condition investigated corresponds to a study performed by TsNIIMASH.¹⁸ The thruster was operated at a flow rate of 3.5 mg/s, a discharge voltage of 300 V and a current of 3 A. The background pressure with the thruster running was 5.9×10^{-3} Pa.

The third flow condition corresponds to a study performed by the University of Tennessee Space Institute (UTSI) and Lockheed Martin Astronautics (LMA).¹⁹ The thruster was operated at a flow rate of 6 mg/s, a discharge voltage of 300 V and a current of 4.5 A. The background pressure with the thruster running was 9.3×10^{-3} Pa.

The D55 has a nozzle-like geometry at the exit, so the plume spreads at the thruster exit. In the present study, we adopt 15 deg as the half angle, and the radial velocity varies linearly across each half of the thruster exit.⁸

The computational grid employed in the present study consists of rectangular cells. The smallest cells are located close to the thruster exit and have a size of 2.5 mm. The largest cells are those close to the edges of the domain and have a size of 10 mm. The domain size is 1.05 m by 0.56 m. The computations presented in the study typically employed 500,000 particles with a total of 60,000 time steps. Table 1 provides a list of the flow conditions assumed at the thruster exit.

III. Results

Overall plasma potential fields obtained with the *Boltzmann model* and the *Detailed model* are presented in Fig 3. For both models, we set 145 V as the plasma potential at the channel exit to obtain good agreement between measured and simulated data, especially for radial profiles of ion current density and axial components of velocity in the very near field plume. Figure 3 shows the *Boltzmann model* results, and Figs. 4a and 4b show the *Detailed model* results without and with the magnetic field, respectively. It is reported that the plasma potential gradient of the *Boltzmann model* and the *Detailed model* are very different.⁹ From Figs. 3 and 4a we can see this feature. From Figs. 4a and 4b, one can see that when the magnetic field is considered, the plasma potential gradients become stronger. It is expected that only electrons are magnetized while ions do not feel any significant effects from the magnetic field. However, plasma flow across the magnetic field under this condition generates additional electric fields which act to increase the total fields. One possible explanation for the trends observed is that the confinement of the electron motion by the magnetic field reduces the electric conductivity which results in increased the electric fields.

A series of probe experiments was performed by Domonkos et al.² in the near field of the D55 plume. The local plasma potential was obtained using an emissive probe and a Langmuir probe; ion current density was obtained using a Faraday probe; and the electron temperature and number density were obtained using a Langmuir probe.

Figures 5a and 5b show radial profiles of plasma potential at axial distances of 10 mm and 50 mm from the thruster exit plane, respectively. Experimental data were measured with respect to the cathode potential of 14 V,² so here we added 14V to the measured data for consistency with the simulation. Close to the thruster, the *Boltzmann model* overpredicts the potential. The *Detailed model* captures the shape quite well although it overpredicts the potential too. However, the result is better than the *Boltzmann model* and if the magnetic field is considered the improvement is remarkable. At 50 mm from the thruster, the *Boltzmann model* still greatly overpredicts the potential. The *Detailed model* without the magnetic field provides improved agreement with the measured data and the magnetic field case gives even better results.

Comparisons between measured data and simulation results for the potential in the far-field plume are shown in Fig. 6. The measured data were obtained by Zakharenkov et al.¹⁸ and the simulations use the second set of operating conditions given in Table 1. At a distance of 500 mm from the thruster, the *Boltzmann model* again greatly overpredicts the potential whereas the *Detailed model* reproduces fairly well the measured profiles.

Ion current density profiles predicted by the simulation are compared with the experimental data² in Figs. 7a and 7b along radial lines located at 10 and 40 mm from the thruster exit plane, respectively. Both the *Boltzmann model* and the *Detailed model* give good prediction at 10 mm. At 40 mm, the models slightly underpredict the results but are still in good agreement. This underprediction of the current density implies a possibility that the simulation overaccelerates ionized particles in the radial direction between 10 and 40 mm from the thruster exit plane. The variation of the ion current density with axial distance from the thruster indicates that the ion flow begins as an annulus and then merges to a cylinder-shaped beam. This feature occurs because the annular ion flow diverges with an angle of 15 degrees which overlaps at the centerline of the thruster as the flow convects downstream. One can see that the magnetic field consideration does not give much change in the ion current density.

Figure 8 shows further comparisons between measured data¹⁸ and simulation results for ion current density in the far-field plume. The *Detailed model* shows better agreement with measurements though both models underpredict the measured values. This underprediction of ion current density over the entire domain suggests that the simulation

may over accelerate ionized particles in the radial direction. This feature is consistent with the comparisons of electron number density shown in Figs. 9 and 10. This feature is discussed later.

Measurements of electron number density² are compared with the simulations for radial profiles at 10 and 50 mm in Figs. 9a and 9b, respectively. The simulation values represent the total charge density obtained from the number densities of the Xe⁺ and Xe⁺⁺ ions. The measured data have an accuracy of ± 50 percent at 10 and 50 mm. Therefore, in the near field, most of the simulation data underpredict the measured values. The peak electron number density measured at both stations is more than double the total charge density assumed in the simulations at the thruster exit plane (see Table 1). Gulczinski et al.²⁰ presented evidence that the Langmuir probe technique leads to high electron number densities. At a distance of 25 cm and 50 cm from the thruster, the Langmuir probe gave six times higher electron number density than the microwave interferometer.¹⁹ One other possible interpretation of these comparisons is that the axial component of electric fields in the simulation is so strong that the acceleration of ions is overestimated in the axial direction. One possible way to address such differences between the model and the measured data would be axial confinement of electrons caused by the magnetic field.

Further comparisons between measured data and simulation results for electron number density in the far-field plume are shown in Figs. 10a and 10b. The measured data were obtained by Gulczinski et al.²⁰ using microwave interferometry and the simulations use the first set of operating conditions given in Table 1. The uncertainty for the measured data is ± 10 percent. The *Detailed model* shows better agreement with the measurements though both models still underpredict the measured values over the entire radial profile. One possible reason for these differences between the *Detailed model* results and the experiment is that the electric fields in the simulation accelerate the ions too much in both the axial and radial directions. This feature also suggests axial confinement of the electrons caused by the magnetic field. It was shown that the axial component of the magnetic field is much smaller than the radial component in SPT-100 thrusters,⁴ although there is no direct evidence that it is true in D55 thrusters. Measurements of the axial component of the magnetic field are required to help resolve this issue, and no such data exist as of now.

Figures 11a and 11b show radial profiles of electron temperature at distances of 10 and 50 mm from the thruster, respectively. The experimental uncertainty is reported to be $\pm 10\%$.² At 10 mm, it is clear from the measurement that there is significant spatial variation in the electron temperature caused by the dynamics of the plasma as it enters the acceleration channel. Electron temperature is constant in the *Boltzmann model* and here we show the value of 10 eV which is used in the simulation. In general, although the *Detailed model* provides reasonable agreement with the

measurements, the radial gradients predicted by the model are smaller than the measured data indicate. These disparities between the models and the measurement indicate that more elaborate thruster exit boundary conditions are needed. In fact, it is known that the *Detailed model* is relatively more sensitive to boundary conditions than the *Boltzmann model*.

Far-field prediction of the electron temperature profiles are presented in Fig. 12. The measured data were obtained by Zakharenkov et al.¹⁸ and the simulations use the second set of operating conditions given in Table 1. It is clearly shown that the *Detailed model* gives good agreement with the measured data in the far field.

Finally, the simulation results are compared with Laser Induced Fluorescence (LIF) measurements of Xe^+ axial velocity component obtained by Keefer et al.¹⁹ in Fig. 13. In Ref. 19, it is explained that the reported velocity data represent the central value of the ion velocity distribution functions detected by the LIF diagnostic. Therefore, for consistency with the experiment, the ion velocity distribution function is calculated throughout the flow field, and the most probable value of the distributions obtained. Figure 13 shows the axial velocity profiles at a radial position of 27.5 mm which is along the thruster channel center. The simulations use the third set of operating conditions given in Table 1. It is clear that the *Boltzmann model* fails to produce sufficient ion acceleration in the near field of the plume. This is an expected result because the plasma potential gradient shown in Fig. 3 is not enough to give ions significant acceleration. As discussed with reference to Fig. 4, the *Detailed model* predicts strong ion acceleration in the near field region and rapidly accelerates the ions from the thruster exit velocity of 15 km/s to a value of about 18 km/s that corresponds to the measured data and the results become slightly better when the magnetic field is considered. The simulation result, however, overestimates the axial velocity at $z=1$ mm. This discrepancy also suggests that improved thruster exit flow conditions are needed.

IV. Conclusion

A hybrid particle-fluid PIC-DSMC model using both a *Detailed model* and the *Boltzmann model* for the fluid electrons was applied to simulate the plume flow from a D55 anode layer Hall thruster. The present model includes the near-field plasma plume region where the magnetic field leaked from the acceleration channel may have a substantial effect on the plasma potential distribution. Analyses of the plasma potential distribution across the magnetic field show that the field significantly affects the profile of the plasma in the *Detailed model*. For instance, in the case of zero magnetic field, the plasma has a potential of about 110V at 10 mm from the thruster exit, while in

the case of a finite magnetic field, the plasma potential is about 80V. Results predicted by the *Detailed model* with the magnetic field are found to be in better agreement with several different sets of experimental data. Generally, the *Detailed model* provided better results than the *Boltzmann model*. The inclusion of the magnetic field in the *Detailed model* gives closer prediction of the plasma potential distribution to the measured one. The *Detailed model* with the magnetic field consideration more accurately predicted the extended ion acceleration region outside the thruster. By comparison, the *Boltzmann model* indicated almost no ion acceleration outside the thruster. The simulation results of the *Detailed model* and the *Boltzmann model* consistently underpredicted the electron number density. This disparity may be caused by the simulated electric fields being too strong and leading to overacceleration of the ions in the axial direction. Future work will involve modeling the D55 thruster plasma to generate improved thruster exit flow conditions.

Acknowledgments

This work is supported by AFOSR Grant FA9550-05-1-0042 with Dr. Mitat Birkan as technical monitor. The authors gratefully acknowledge the contributions to this work by Dr. Chunpei Cai for discussions.

References

- ¹Marrese, C. M., Frisbee, R., Sengupta, A., Cappelli, M. A., Tverdoklebov, S., Semenkin, S., and Boyd, I. D., "Very High I_{sp} Thruster with Anode Layer (VHITAL): An Overview," *AIAA Paper* 2004-5910, July 2004.
- ²Domonkos, M. T., Marrese, C. M., Haas, J. M., and Gallimore, A. D., "Very Near-Field Plume Investigations of the D55," *AIAA Paper* 97-3062, July 1997.
- ³Oh, D. Y., Hastings, D. E., Marrese, C. M., Haas, J. M., Gallimore, A. D., "Modeling of Stationary Plasma Thruster-100 Thruster Plumes and Implications for Satellite Design", *Journal of Propulsion and Power*, Vol. 15, No 2, 1999, pp. 345-357.
- ⁴Keidar, Michael, Boyd, I. D., "Effect of a Magnetic Field on the Plasma Plume from Hall Thrusters", *Journal of Applied Physics*, Vol. 86, 1999, pp. 4786-4791.
- ⁵Bird, G. A., *Molecular Gas Dynamics and the Direct Simulation of Gas Flows*, Oxford Press, New York, 1994.
- ⁶Birdsall, C. K., and Langdon, A. B., *Plasma Physics Via Computer Simulation*, Adam Hilger, New York, 1991.
- ⁷Keidar, M., Choi, Y., and Boyd, I. D., "Modeling a Two-Stage High-Power Bismuth Anode Layer Thruster and its Plume," *IEPC Paper* 2005-045, October 2005.

- ⁸ Boyd, I. D., "Computation of the Plume of an Anode-Layer Hall Thruster," *Journal of Propulsion and Power*, Vol. 16, No. 5, 2000, pp. 902-909.
- ⁹ Boyd, I. D. and Yim, J. T., "Modeling of the Near Field Plume of a Hall Thruster," *Journal of Applied Physics*, Vol. 95, 2004, pp. 4575-4584.
- ¹⁰ Cai, C., and Boyd, I. D., "3D Simulation of Plume Flows from a Cluster of Plasma Thrusters," *AIAA Paper* 2005-4662, July 2005.
- ¹¹ Dietrich, S. and Boyd, I. D., "Scalar and Parallel Optimized Implementation of the Direct Simulation Monte Carlo Method", *J. of Computational Physics*, Vol. 126, 1996, pp. 328-342.
- ¹² Ahedo, E., Martinez-Cerezo, P., and Martinez-Sanchez, M., "One-dimensional Model of the Plasma Flow in a Hall Thruster," *Physics of Plasma*, Vol. 8, 2001, pp. 3058-3068.
- ¹³ Braginsky, S. I., in *Reviews of the Plasma Physics* edited by Leontovich, M. A., (Consultants Bureau, New York, 1965), Vol. 1.
- ¹⁴ Mitcher, M., and Kruger, C. H., *Partially Ionized Gases*, Wiley, 1973.
- ¹⁵ Pullins, S. H., Chiu, Y., Levandier, D. J., and Dresseler, R. A., "Ion Dynamics in Hall Effect and Ion Thruster – Xenon Symmetric Charge Transfer," *AIAA Paper* 2000-0636, January 2000.
- ¹⁶ Miller, S., Levandier, D. J., Chiu, Y., and Dresseler, R. A., "Xenon Charge Exchange Cross Sections for Electrostatic Thruster Models," *Journal of Applied Physics*, Vol. 19, 2002, pp. 984-991.
- ¹⁷ Semenkin, A., Kochergin, A., Garkusha, V., Chislov, G., Rusakov, A., Tverdoklebov, S., and Sota, C., "RHETT/EPDM Flight Anode Layer Thruster Development," *IEPC Paper* 97-106, August 1997
- ¹⁸ Zakharenkov, L., Semenkin, A. V., and Lebedev, Y. V., "Measurement Features and Results of TAL D-55 Plume," *IEPC Paper* 2005-184, October 2005.
- ¹⁹ Keefer, D., Wright, N., Hornkohl, J. O., and Bangasser, J., "Multiplexed LIF and Langmuir Probe Diagnostic Measurements in the TAL D-55 Thruster," *AIAA Paper* 97-2425, July 1999.
- ²⁰ Gulczinski, F. S., Gallimore, A. D., Carlson, D. O., and Gilchrist, B. E., "Impact of Anode Layer Thruster Plumes on Satellite Communications," *AIAA Paper* 97-3067, July 1997.

Table 1 Flow properties assumed at thruster exit plane

Experiment	species	n, m^{-3}	T, K	U, m/s
Michigan	Xe	1.1×10^{18}	750	281
	Xe ⁺	4.0×10^{17}	46,400	15,000
	Xe ⁺⁺	1.0×10^{17}	46,400	21,300
TsNIIMASH	Xe	2.8×10^{18}	750	281
	Xe ⁺	2.7×10^{17}	46,400	15,000
	Xe ⁺⁺	6.6×10^{16}	46,400	21,300
UTSI & LMA	Xe	8.9×10^{19}	750	281
	Xe ⁺	4.0×10^{17}	46,400	15,000
	Xe ⁺⁺	1.0×10^{17}	46,400	21,300

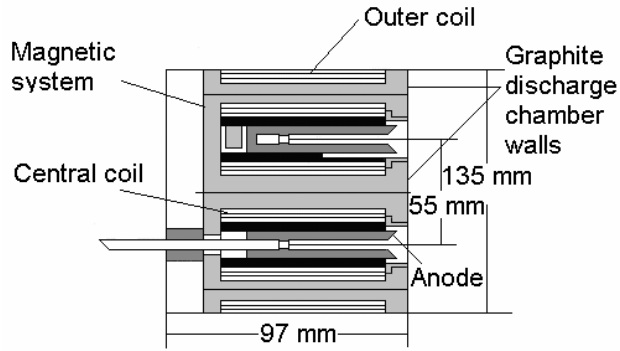


Figure 1. Schematic of the D55 anode-layer Hall thruster.

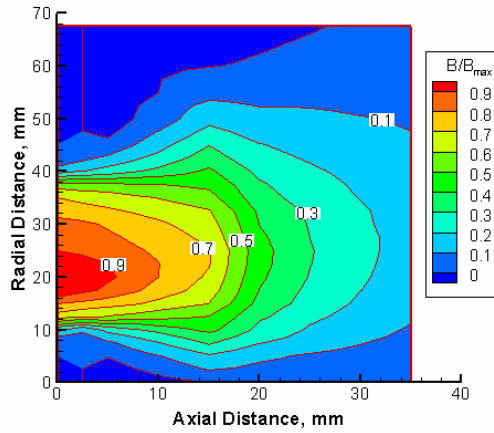


Figure 2. Magnetic field profiles.

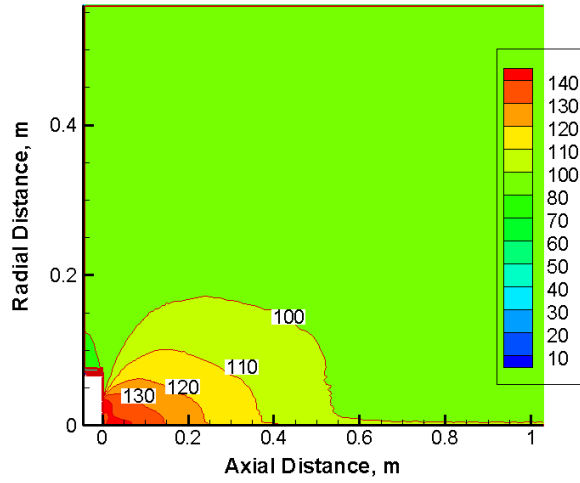
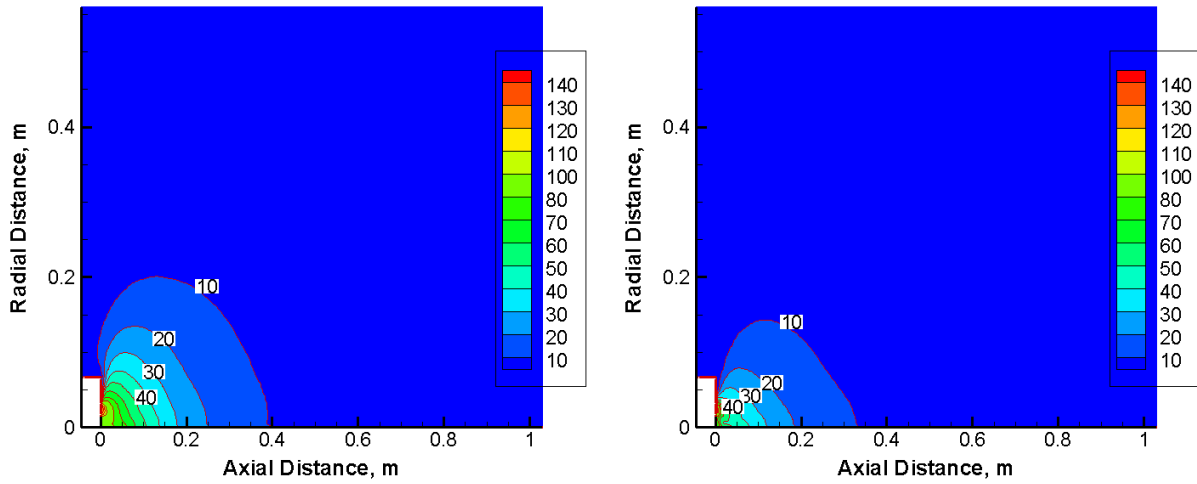


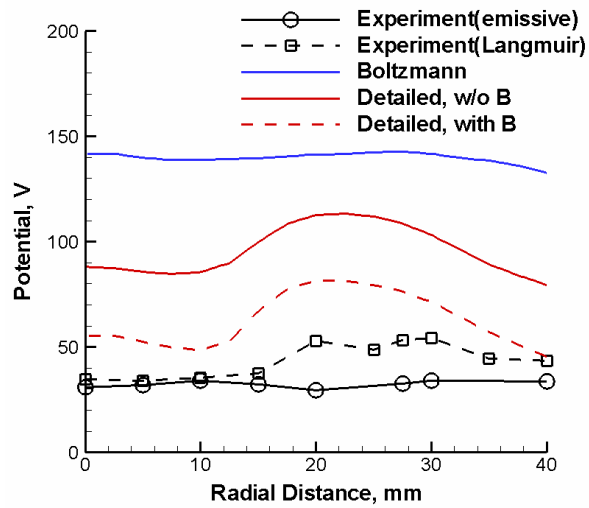
Figure 3. Contours of plasma potential (in V), the Boltzmann model



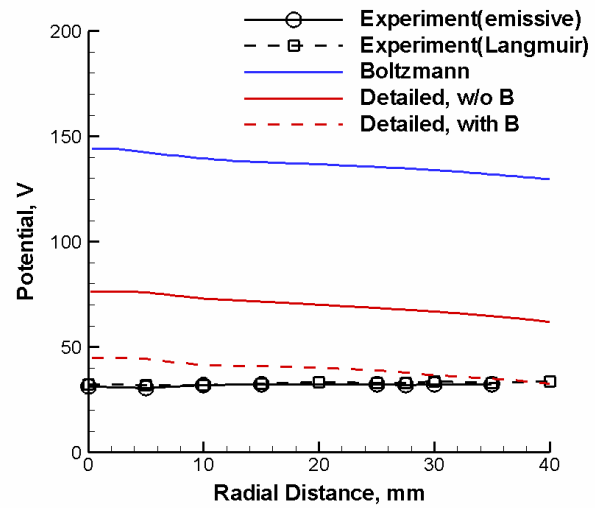
(a) without magnetic field

(b) with magnetic field

Figure 4. Contours of plasma potential (in V), the Detailed model



(a) 10 mm from the thruster exit plane.



(b) 50 mm from the thruster exit plane.

Figure 5. Radial profiles of plasma potential.

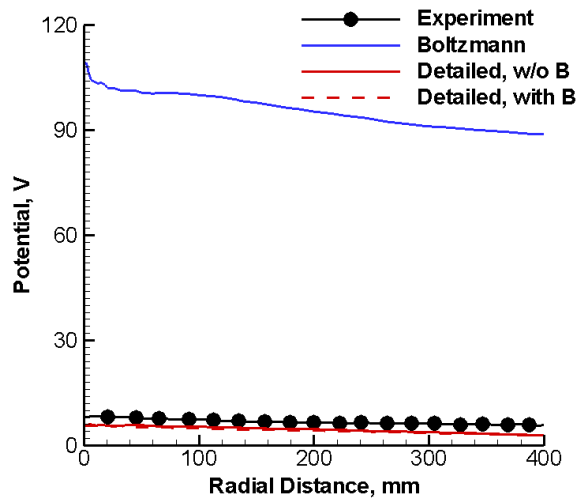
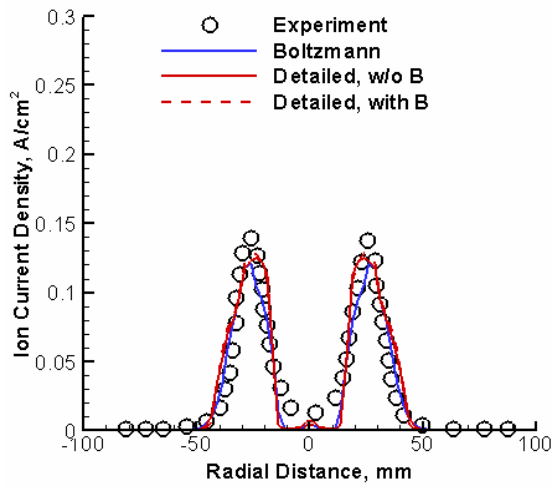
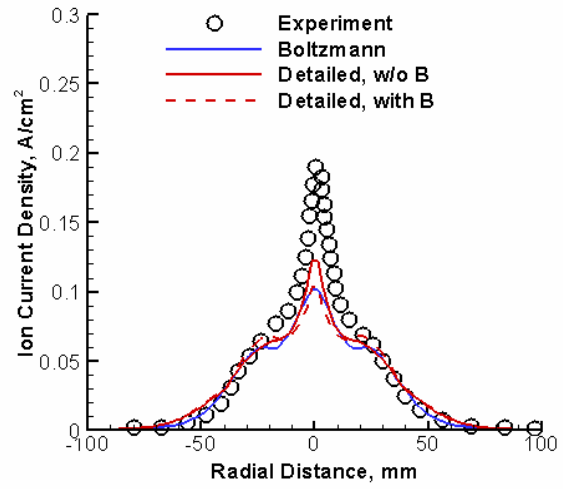


Figure 6. Radial profiles of plasma potential at 500 mm from the thruster exit plane



(a) 10 mm from the thruster exit plane.



(b) 40 mm from the thruster exit plane.

Figure 7. Radial profiles of ion current density

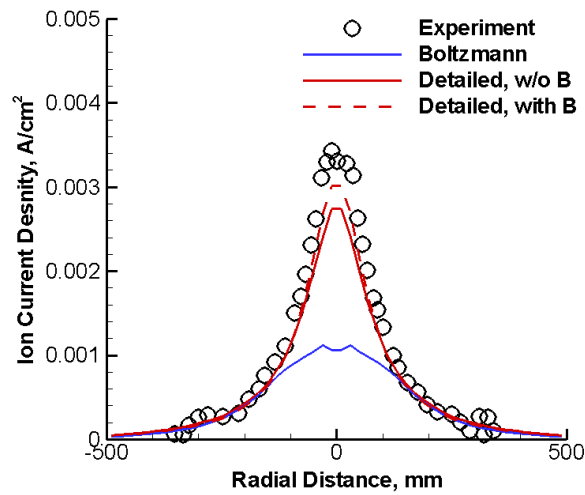
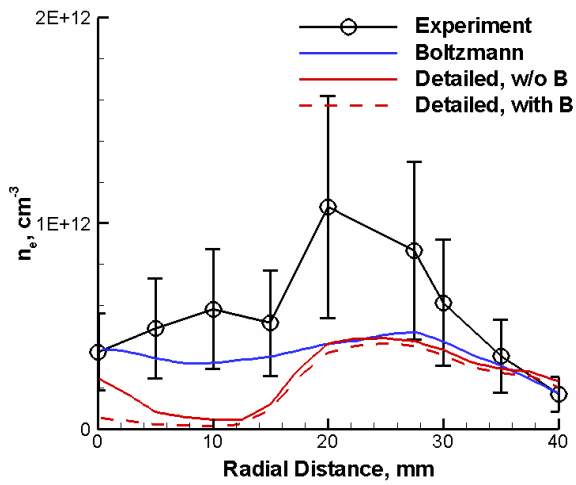
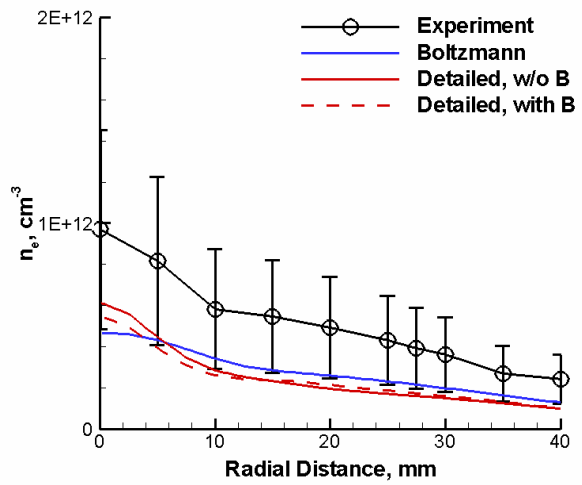


Figure 8. Radial profiles of ion current density at 500 mm from the thruster exit plane

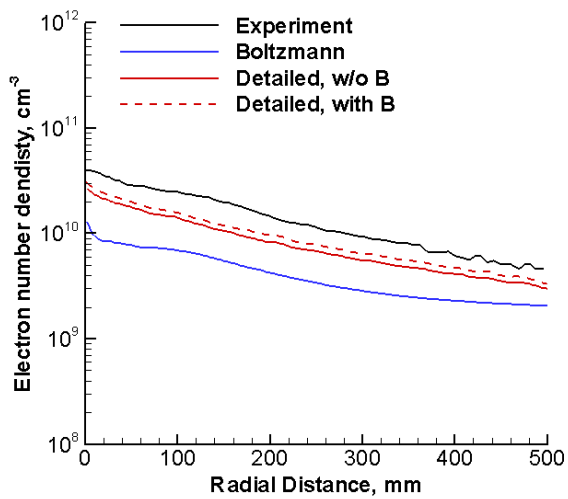


(a) 10 mm from the thruster exit plane.

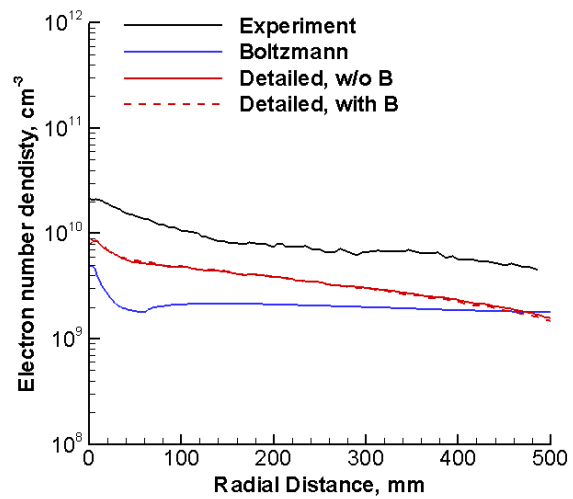


(b) 50 mm from the thruster exit plane.

Figure 9. Radial profiles of electron number density

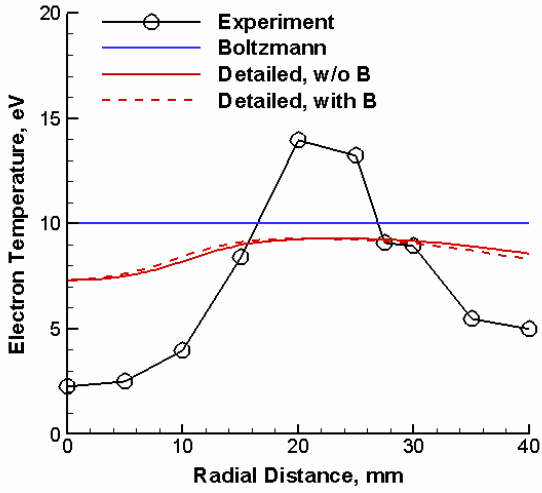


(a) 500 mm from the thruster exit plane.

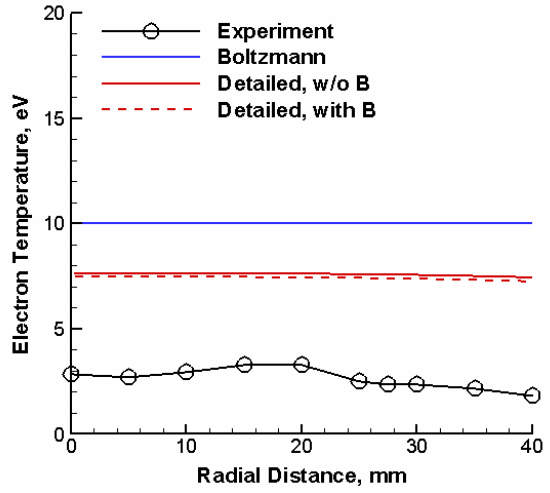


(b) 1000 mm from the thruster exit plane.

Figure 10. Radial profiles of electron number density



(a) 10 mm from the thruster exit plane.



(b) 50 mm from the thruster exit plane.

Figure 11. Radial profiles of electron temperature

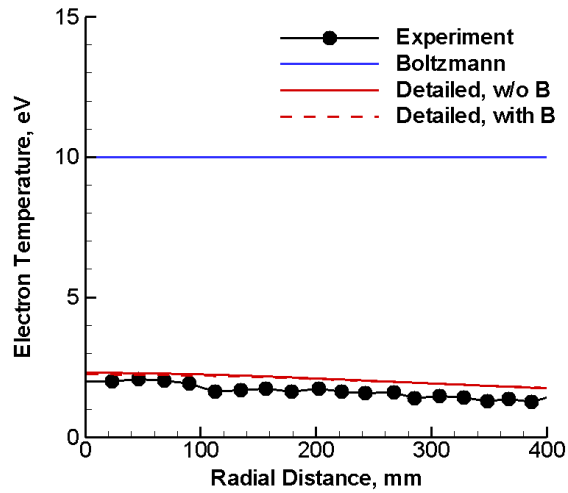


Figure 12. Radial profiles of electron temperature at an axial distance of 500 mm from the thruster

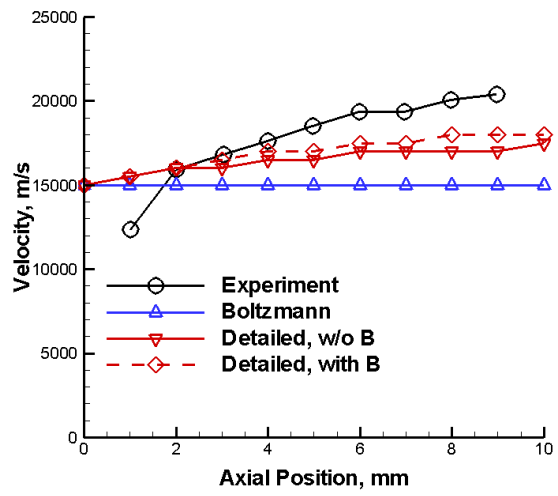


Figure 13. Axial components of ion velocity at a radial position of 27.5 mm.